



1 **Development of a hydrological ensemble prediction system and a**  
2 **visualization approach for improved interpretation during typhoon**  
3 **events**

4 Sheng-Chi Yang<sup>1</sup>, Tsun-Hua Yang<sup>1</sup>, Ya-Chi Chang<sup>1,\*</sup>, Cheng-Hsin Chen<sup>1</sup>, Mei-Ying  
5 Lin<sup>1</sup>, Jui-Yi Ho<sup>1</sup> and Kwan-Tun Lee<sup>1,2</sup>

6 <sup>1</sup>*Taiwan Typhoon and Flood Research Institute (TTFRI), National Applied Research Laboratories*  
7 *(NARLabs), Taipei, Taiwan*

8 <sup>2</sup>*Department of River and Harbor Engineering, National Taiwan Ocean University, Keelung, Taiwan*

9 *\*Correspondence to: 11 F, No. 97, Sec. 1, Roosevelt Rd., Zhongzheng Dist., Taipei City 10093, Taiwan*  
10 *(R.O.C.)*

11 *E-mail: rachel.ev91@gmail.com*

12

13 **ABSTRACT**

14 Typhoons are accompanied by heavy rainfall and cause loss of life and property.  
15 Hydrological ensemble prediction systems can provide decision makers with  
16 hydrological information, such as peak stage and peak time, with some lead time. This  
17 information assists decision makers in taking the necessary measures to prevent and  
18 mitigate disasters. This study proposes a hydrological ensemble prediction system that  
19 includes numerical weather models that perform rainfall forecasts and hydrologic  
20 models that produce assessments of surface runoff and the associated flooding.  
21 However, the spatiotemporal uncertainty associated with the numerical models and the  
22 difficulty in interpreting the model results hinder effective decision making during  
23 emergency response situations. Thus, this study also presents an extension of the 'Peak-



24 Box' visualization methodology that assists in interpreting the forecast results for  
25 operational purposes. A small watershed with area of 100 km<sup>2</sup> and four typhoons that  
26 occurred from 2012 to 2015 were selected to evaluate the performance of these tools.  
27 The results showed that the modified visualization approach improved the intelligibility  
28 of forecasts of the peak stages and peak times compared to that of approaches  
29 previously described in the literature. The new approach includes all available forecasts  
30 to increase the sample size. The capture rate is greater than 50%, which is considered  
31 practical for decision makers. The proposed system and the modified visualization  
32 approach have demonstrated their potential for both decreasing the uncertainty of  
33 numerical rainfall forecasts and improving the performance of flood forecasts.

34

35 **KEY WORDS** Hydrological ensemble prediction system; peak flow; decision support;  
36 visualization.

37



38

## 1. INTRODUCTION

39 Numerical weather prediction (NWP) models generate different precipitation  
40 forecasts for specified locations and times due to the incompleteness of the input  
41 observations, the approximate nature of the forecast models and their parameterizations,  
42 and the random errors that result from perturbing the initial atmospheric conditions  
43 (Palmer, 2001; Hostache et al., 2011). Ensemble prediction systems (EPSs), which  
44 consist of an adequate number of equiprobable NWP models, have been established to  
45 provide probabilistic precipitation forecasts instead of a single deterministic forecast  
46 (Cloke and Pappenberger, 2009). An EPS provides predictions with greater skill than  
47 those obtained from individual runs of NWP models or deterministic model runs,  
48 especially for longer lead times (Demeritt et al., 2007; Cuo et al., 2011).

49 A hydrological ensemble prediction system (HEPS) is an integrated system that  
50 couples an EPS with catchment-scale hydrological models to provide flood forecasts  
51 with sufficient lead time. The importance of such systems in disaster mitigation, water  
52 resource management, and hydropower dam and lake operation is growing  
53 (Pappenberger et al., 2005; Cloke and Pappenberger, 2009; Zappa et al., 2010, 2013;  
54 Yang and Yang, 2014). However, uncertainties stemming from factors including  
55 boundary conditions, initial conditions, and model parameter values affect the forecast  
56 accuracy of these systems. The precipitation forecasts of NWP models dominate the



57 overall uncertainty of these systems (Zappa et al., 2011; Rossa et al., 2011). It is  
58 necessary to develop guidelines and tools for communicating the uncertainties  
59 associated with complex HEPSs (e.g., Jaun et al., 2008; Thielen et al., 2009; Bartholmes  
60 et al., 2009; Todini, 2009; Bruen et al., 2010; Renard et al., 2010; Thirel et al., 2010;  
61 Zappa et al., 2010, 2013; Frick and Hegg, 2011; Pappenberger et al., 2011a, 2011b;  
62 Fundel and Zappa, 2011; Pappenberger et al., 2013).

63 Effective communication of ensemble forecasts means that clear expression of the  
64 uncertainties associated with HEPS is important so that end-users can easily respond to  
65 the information provided during operations (Demeritt et al., 2010; Ramos et al., 2010;  
66 Pappenberger et al., 2013; Zappa et al., 2013; Pagano et al., 2014). Pagano et al. (2014)  
67 noted that defining effective methods for the communication of ensemble forecasts is a  
68 challenge for future operational river forecasting and represents a future research  
69 opportunity. Pappenberger et al. (2013) argued that the uncertainty information  
70 provided by HEPSs sometimes results in resistance on the part of the public if experts  
71 or nonexperts cannot easily understand the information provided. At present, HEPSs  
72 still rely on conventional visualization techniques, such as ‘spaghetti diagrams’ or box  
73 plots, to display the distributions of forecast results. Pappenberger et al. (2013) focused  
74 on expert users of HEPSs and the communication among these experts and identified  
75 key information for the public, such as discharge, lead time, warning levels, return



76 periods, worst/best scenario, etc. Zappa et al. (2013) proposed the ‘Peak-Box’  
77 visualization approach to support the interpretation and verification of HEPS results.  
78 This approach has been used to obtain quantitative and qualitative insights, such as the  
79 timing, water level, and discharge associated with peak flow. This information is crucial  
80 for end-users and decision makers. Zappa et al. (2013) applied an operational HEPS,  
81 namely, the IFKIS-HYDRO hydrological nowcasting system, to five different basins in  
82 Switzerland to evaluate the performance of the ‘Peak-Box’ methodology. The sizes of  
83 the basins ranged from 186 km<sup>2</sup> to 1696 km<sup>2</sup>. The study found that, of 485 operational  
84 forecasts performed from June 2007 through November 2008, 30% to 55% of the  
85 observed peaks fell outside the ‘Peak-Box’.

86 Typhoons are common natural events that cause severe damage in countries at the  
87 edge of the northwestern Pacific Ocean, such as Japan, the Philippines, and Taiwan. For  
88 example, based on records covering 1958 to 2010, an average of 3.4 typhoons affect  
89 Taiwan annually, and these events cause an annual average loss of more than 500  
90 million U.S. dollars (Li et al., 2004). Typhoon-related flood events cause these losses.  
91 If they provide early warnings with sufficient lead time, flood forecasts from a HEPS  
92 can help authorities prepare disaster prevention and mitigation measures. A customized  
93 visualization method for typhoons is also necessary to make the ensemble flood  
94 forecasts generated by HEPS meaningful for emergency responders. Therefore, this



95 study presents a HEPS that can provide ensemble flood forecasts during typhoon events  
96 and proposes a customized visualization approach especially for typhoons to simplify  
97 the forecast information. This approach is an extension of the one presented by Zappa  
98 et al. (2013); it has been modified to increase the percentage of observed peaks that fall  
99 within the predicted range during typhoon events. The remainder of this paper is  
100 organized as follows. Section 2 includes the details of the proposed HEPS. Section 3  
101 briefly describes the study area and typhoon events used in the study. Section 4  
102 compares the original ‘Peak-Box’ approach with the proposed extended version. Finally,  
103 Sect. 5 and 6 present the results, discussion, and conclusions.

## 104 2. SETUP OF THE HYDROLOGICAL ENSEMBLE PREDICTION 105 SYSTEM

106 This study proposes a HEPS that integrates various models. These models include  
107 NWP models that provide ensemble precipitation forecasts, a rainfall-runoff model that  
108 generates upstream boundary conditions, a storm surge model that generates  
109 downstream boundary conditions, and a flood routing model that simulates river flows.  
110 The data processing is shown in Figure 1. The HEPS produces ensemble flood forecasts  
111 with a 72-hour lead time four times a day. The models used in the HEPS are described  
112 in the following subsections.



113 *2.1 Ensemble precipitation forecasts*

114       The Taiwan Cooperative Precipitation Ensemble Forecast Experiment (TAPEX)  
115 began in 2010. It is a collective effort among academic institutes and government  
116 agencies, such as the National Taiwan University, the National Central University, the  
117 National Taiwan Normal University, the Chinese Culture University, the Central  
118 Weather Bureau (CWB), the National Center for High-Performance Computing, the  
119 Taiwan Typhoon and Flood Research Institute (TTFRI), and the National Science and  
120 Technology Center for Disaster Reduction. TAPEX is the first attempt to design a high-  
121 resolution (5-km) numerical ensemble model in Taiwan. This effort applies various  
122 NWP models, such as the Weather Research and Forecasting Model (WRF), the Fifth-  
123 Generation Penn State/NCAR Mesoscale Model (MM5), the Cloud-Resolving Storm  
124 Simulator (CReSS), and the Hurricane Weather Research and Forecasting Model  
125 (HWRF). It also considers different setups in terms of the model initial conditions, data  
126 assimilation processes and model physics. TAPEX generates four runs a day and  
127 provides ensemble predictions of the wind and pressure fields and quantitative  
128 estimates of precipitation with a lead time of 72 hours. Further information can be found  
129 in Hsiao et al. (2013). A typhoon's average impact duration is 73.68 hours (Huang et  
130 al., 2012) and the average lag between observed peak precipitation and flooding in  
131 Taiwan is between 2 and 10 hours (Jang et al., 2012). This study focuses on a one-way



132 coupling in which TAPEX provides rainfall forecast to the rainfall-runoff model;  
133 feedbacks from the rainfall-runoff model to TAPEX are not considered.

#### 134 *2.2 Rainfall-runoff model*

135 The HEPS uses the surface runoff forecast generated by a kinematic-wave-based  
136 geomorphologic instantaneous unit hydrograph model (the KW-GIUH model) as its  
137 upstream boundary condition. The KW-GIUH model, which was developed by Lee and  
138 Yen (1997), can reflect the effects of watershed geomorphology, land cover conditions,  
139 soil characteristics and rainfall intensity on runoff. It has been successfully applied to  
140 many Taiwanese catchments (Lee et al., 2001; 2006).

#### 141 *2.3 Storm surge model*

142 Storm surges are abnormal increases in water levels above those expected from  
143 astronomical tides. They are generated by strong winds and atmospheric pressure  
144 changes and affect water levels downstream (near estuaries) during typhoons. The  
145 HEPS uses the storm surge and tide forecasts generated by the Princeton Ocean Model  
146 (POM) and the TOPEX-POSEIDON global tidal model (TPXO6.2) as downstream  
147 boundary conditions. The POM model, which was developed by Blumberg and Mellor  
148 (1987), is a three-dimensional, nonlinear, primitive equation finite difference ocean  
149 model. It has been applied to simulate a wide range of ocean problems, including  
150 coastal storm surge in Taiwan (Ou et al., 2008; Chiou, 2010). In this study, the TAPEX





151 model provides ensemble pressure field and wind field forecasts to POM and the  
152 TPXO6.2 model and obtains tidal level predictions. As with TAPEX, it generates four  
153 runs a day, and each run has a 72-hour lead time.

#### 154 *2.4 Flood routing model*

155 The Numerical Model Simulating Water Flow and Contaminant and Sediment  
156 Transport in WAterSHed Systems of 1D Stream/River Networks, 2D Overland  
157 Regimes, and 3D Subsurface Media (WASH123D) was developed by Yeh et al. (1998)  
158 to simulate one-dimensional channel networks, two-dimensional overland flow, and  
159 three-dimensional variably saturated subsurface flow. It has been applied successfully  
160 in Taiwan and around the world, and it was chosen by the US Army Corps of Engineers  
161 as the core computational code used in modeling the Lower East Coast (LEC) Wetland  
162 Watershed (e.g., Yeh et al., 2006; Yeh and Shih., 2011; Shih et al., 2012; Hsiao et al.,  
163 2013). The HEPS uses the one-dimensional channel model of WASH123D as its flood  
164 routing model to simulate water stages in rivers.

### 165 3. STUDY AREA AND TYPHOON EVENTS

#### 166 *3.1 Study area*

167 This study selected the Yilan River in northeastern Taiwan as the study area  
168 (Figure 2). The river flows through the city of Yilan and has a main stream length of  
169 approximately 24.4 km and a watershed area of 149.06 km<sup>2</sup>. It has four main tributaries,



170 which are the Wushi River, the Dahu River, the Dajiao River and the Xiaojiao River.  
171 The Water Resource Agency (WRA) and TTFRI have selected this river as one of two  
172 watersheds where long-term monitoring experiments are being carried out (the other is  
173 the Dianbao Creek basin in southwestern Taiwan). The purpose of the experimental  
174 watersheds is to generate long-term and high-density hydrological monitoring data that  
175 can be used for scientific studies, including the development of hydrological and  
176 hydraulic models and the study of environmental changes. In total, 11 rainfall gauging  
177 stations, 16 water-stage gauging stations, five river-velocity gauging stations, and 36  
178 inundation-depth gauging stations have been installed in the Yilan River Basin. Figure  
179 2 shows the locations of the water-stage and rainfall gauging stations that collected the  
180 data that we used in this study. The monitoring data have been carefully collected and  
181 processed. For full information and to download the available data, please refer to the  
182 official website (<http://wraew.tfri.narl.org.tw/index.php>).

183 TAPEX provides 72-hour rainfall forecasts for five rainfall gauges in the upstream  
184 portion of the Yilan River Basin. The KW-GIUH model calculates the surface runoff  
185 and estimates river flow at the Hsincheng and Yuanshan Bridges. This study uses the  
186 POM and TPXO6.2 models to forecast the tides at Suao and to estimate the water stages  
187 at the Kemalan Bridge. WASH123D then generates ensemble flow forecasts using  
188 flows at the bridges mentioned above as the upstream boundary condition and the water



189 stage at the Kemalan Bridge as the downstream boundary condition. The detailed  
190 locations of these places are shown in Figure 2.

### 191 *3.2 Typhoon events*

192 Figure 3 shows the tracks of the different typhoons that have affected Taiwan,  
193 according to historical records (Huang et al., 2012). Of the ten categories, Type-2 and  
194 Type-3 typhoons account for approximately 28% of all typhoons and bring heavy  
195 rainfall to the Yilan River Basin. For instance, a rainfall of 158 mm in 4 hours was  
196 observed at rainfall gauging station C1U610 (shown in Figure 2) during Typhoon  
197 Soulik. Table 1 shows all of the typhoons that invaded Taiwan from 2012 through 2015.  
198 Five of these events are Type-2 and Type-3 typhoons, which have the biggest impact  
199 on the Yilan River Basin. Therefore, this study selected the typhoons Saola (2012),  
200 Soulik (2013), Soudelor (2015), and Dujan (2015) to calibrate the HEPS and test its  
201 performance. Typhoon Matmo, a Type-3 typhoon that occurred in 2014, was not  
202 included due to its weak intensity. This study used historical observations of rainfall,  
203 river stage, and tide to validate the parameters in the proposed HEPS.

## 204 4. A VISUALIZATION APPROACH FOR SUPPORTING THE 205 INTERPRETATION OF OPERATIONAL ENSEMBLE PEAK-



206                                   FLOW FORECASTS DURING TYPHOON EVENTS

207             This study modified the ‘Peak-Box’ approach originally proposed by Zappa et al.  
208 (2013) to provide better communication of HEPS forecasts during typhoon events.  
209 Figure 4 compares the two approaches, and the modifications are described in detail  
210 below. The purpose of the modifications is to develop a visualization approach that  
211 simplifies the ensemble flow forecast information for use in formulating emergency  
212 responses during typhoon events.

213 a. **Remove the horizontal and the vertical lines.** The horizontal and vertical lines  
214 that indicate the medians of ensemble forecasts in the original ‘Peak-Box’ approach  
215 are removed to prevent some information from being misused. Although  
216 uncertainties exist in the HEPS, Pappenberger et al. (2013) noted a considerable  
217 desire on the part of end-users to reduce probabilistic forecasts to deterministic  
218 actions. The two lines may lead end-users to believe that the information provided  
219 represents a single deterministic forecast, rather than a probabilistic one.

220 b. **Remove the outer rectangle.** In the original ‘Peak-Box’ approach, two rectangles  
221 are displayed. The outer rectangle is the ‘Peak-Box,’ which highlights all  
222 possibilities from the ensemble forecast, and the inner rectangle is the ‘IQR-Box’  
223 that emphasizes the 25th and 75th percentiles of the peak times and peak discharges  
224 of the ensemble forecast. Zappa et al. (2013) argued that the outer rectangle



225 provides the forecaster with additional information. However, this argument does  
226 not hold during typhoons, when the availability of too much data may obscure  
227 critical information. Therefore, only one rectangle is shown in the study. This  
228 rectangle indicates where the observed peak stage is likely to occur.

229 c. **Use the mean and the standard deviation to define the rectangle.** This study  
230 defines an ‘SD-Box’ that uses the mean ( $\mu$ ) and the standard deviation ( $\sigma$ ), instead  
231 of the first and third quartiles, to define the enveloping rectangle. As shown in the  
232 right panel of Figure 4, the lower left coordinate of the ‘SD-Box’ is defined as the  
233 mean peak time minus one standard deviation ( $\mu_t - \sigma_t$ ) and the mean peak stage  
234 minus one standard deviation ( $\mu_h - \sigma_h$ ) produced by all of the ensemble members.  
235 The upper right coordinate is defined as the mean peak time plus one standard  
236 deviation ( $\mu_t + \sigma_t$ ) and the mean peak stage plus one standard deviation ( $\mu_h +$   
237  $\sigma_h$ ) of all of the ensemble members. In principle, the ‘IQR-Box’ should contain  
238 25% (50% of the peak discharge times and 50% of the peak times) of all forecasts.  
239 In practice, it contained from 12.5% to 37.5%, due to the distribution of ensemble  
240 members (Zappa et al., 2013). Using the mean and the standard deviation (the ‘SD-  
241 Box’) results in a larger area, includes 46.60% of the ensemble forecasts (68.27%  
242 of peak water level times and 68.27% of the peak times) and has a greater chance  
243 of including the observed peaks.



244 d. **Include all forecasts with different lead times in the rectangle.** Descriptive  
245 statistics, such as the quartile deviation and the standard deviation, are susceptible  
246 to outliers when calculated using insufficient sample sizes. Adding extra ensemble  
247 members to produce more forecasts consumes computer resources. Yang et al.  
248 (2016) showed that the performance of NWP models is independent of the length  
249 of the lead time during typhoon events. Therefore, in order to expand the sample  
250 size, this study includes present ( $t$ ) and previous forecasts ( $t-1$ ,  $t-2$ ,  $t-3$ ...  $t-n$ , where  
251  $n$  is the number of available forecasts when the system is initiated) to provide  
252 ensemble flow forecasts. As shown in the right panel of Figure 4, the green area  
253 illustrates the ‘SD-Box’. The black and gray solid dots represent the current and  
254 previous peak-flow forecasts, respectively.

## 255 5. RESULTS AND DISCUSSION

### 256 5.1 Performance evaluation criteria

257 This study applied two performance measures, the root mean square error (RMSE)  
258 and the skill-spread ratio, to evaluate the proposed HEPS performance. For a well-  
259 designed HEPS, the spread of ensemble forecasts will be large enough to cover the  
260 prediction uncertainty. This statement implies that the spread should be the same as or  
261 larger than the RMSE. The RMSE, which is commonly referred to as skill, measures  
262 the difference between the observations and the ensemble mean without considering



263 the direction. The closer the RMSE is to zero, the better the ensemble mean is as a  
264 forecast. The RMSE is defined as follows:

$$265 \quad \text{RMSE} = \sqrt{(O_{peak} - \mu)^2} \quad (1)$$

$$266 \quad \mu = \frac{1}{m} \sum_{i=1}^m P_{peak,i} \quad (2)$$

$$267 \quad \sigma = \sqrt{\frac{1}{m} \sum_{i=1}^m (P_{peak,i} - \mu)^2} \quad (3)$$

268 where  $\mu$  is the ensemble mean of ensemble peak-flow forecasts;  $O_{peak}$  is the observation  
269 of peak flow;  $P_{peak,i}$  is the prediction of peak flow of the  $i$ th member;  $m$  is the number of  
270 ensemble members; and  $\sigma$  is the standard deviation of ensemble peak-flow forecasts.

271 The skill-spread score (hereinafter referred to as the score), which ranges from  
272 zero to infinity, is the ratio of the standard deviation of the ensemble peak-flow forecasts  
273 to the RMSE (Wilks, 2006). Scores less than one mean that the spread of the ensemble  
274 forecasts is large enough to cover the prediction uncertainty. It is defined as follows:

$$275 \quad \text{Score} = \frac{\text{RMSE}}{\sigma} \quad (4)$$

## 276 5.2 Model calibration and validation

277 Two parameters in the proposed HEPS KW-GIUH model have been calibrated  
278 using in situ observations made during typhoon events. These parameters are the  
279 roughness coefficient for overland flow ( $n_0$ ) and the roughness coefficient for channel



280 flow ( $n_c$ ). The proposed HEPS used data from five rainfall gauges, including LTGX,  
281 YSGZ, C1U610, C0U520 and C1U630 (see Figure 2 for locations), and the Thiessen  
282 polygon method (Thiessen, 1911) to estimate the hourly spatial-average rainfall  
283 intensities in order to provide rainfall input data to the KW-GIUH model. The  
284 topographic data used in KW-GIUH are contained within a digital elevation model with  
285 a resolution of 5 m obtained using aerial photographs. Kuo et al. (2016) used in situ  
286 observations of flow discharges made at the Hsincheng and Yuanshan Bridges during  
287 Typhoons Saola, Soulik, and Soudelor to calibrate the parameters of the KW-GIUH  
288 model. Figure 5 shows that the percent errors in the peak discharges of the selected  
289 typhoons were 4.59%, 2.07%, and -5.89% at the Hsincheng Bridge, and 14.88%, 5.28%,  
290 and -3.05% at the Yuanshan Bridge, respectively. All of the errors in the peak times  
291 were less than one hour. The results show that the KW-GIUH model is capable of  
292 providing confident predictions for peak time, as well as peak discharge.

293 The WASH123D model adopted the most recent available cross-sectional  
294 bathymetry of the Yilan River, which was measured in 2010, as its input topography  
295 data. The upstream boundary of the model is set at the Hsincheng and Yuanshan Bridges,  
296 and the downstream boundary of the model is set at the Kemalan Bridge. Field  
297 measurements at the Hsincheng and Yuanshan Bridges from Kuo et al. (2016) and  
298 observed water stages at the Kemalan Bridge were used as the upstream and





299 downstream boundary conditions, respectively. Field hourly records of water-stage at  
300 the Zhongshan, Leawood, and Jhuangwei Bridges were used to calibrate the value of  
301 Manning's roughness coefficient ( $n$ ) in the WASH123D model and to validate the  
302 performance of the model. Figure 6 shows that the percent errors in the peak stage for  
303 Typhoons Saola, Soulik, and Soudelor, were 2.1%, 5.7%, and 10.6% at Zhongshan,  
304 12.9% and 2.2% at Leawood, and 7.4%, 6.0%, and 2.1% at Jhuangwei, respectively.  
305 There was one data gap at Leawood due to incomplete data collection during Typhoon  
306 Soudelor. Nevertheless, all of the errors in the peak times were less than one hour. The  
307 results show that WASH123D is capable of providing confident predictions of peak  
308 times, as well as peak stages.

309 *5.3 Comparison of enveloping rectangles defined using the 'SD-Box' and the 'IQR-Box'*  
310 *methods for supporting the interpretation of ensemble peak-flow results*

311 The proposed HEPS initiates when CWB issues a sea warning and ends when the  
312 next ensemble forecast is six hours less than the left edge of the 'SD-Box'. In that regard,  
313 93 forecasts are available for the four selected typhoons. Table 2 compares the forecast  
314 peak stages and peak times between the 'SD-Box' and 'IQR-Box' approaches at the  
315 Zhongshan, Leawood, and Zhuangwei Bridges. Scores were not calculated for the  
316 Leawood Bridge during Typhoon Soudelor due to the lack of complete observations.  
317 The scores that are less than one in the table are highlighted. These values indicate that



318 the spread of the ensemble members is large enough to contain the prediction  
319 uncertainty. The rectangles defined using the ‘IQR-Box’ method contain 33.3% (31/93)  
320 and 52.6% (49/93) of the observed peaks in stage and timing, respectively. Using the  
321 ‘SD-Box’ improves the capture rate to 51.6% (48/93) and 64.5% (60/93) for stage and  
322 timing, respectively. Among all of the forecasts, there is only one forecast for which the  
323 ‘IQR-Box’ score is less than one, and the score of the ‘SD-Box’ is not. This situation  
324 occurs at the Zhuangwei Bridge during Typhoon Soudelor. However, the score for the  
325 ‘SD-Box’ method is still very close to one (1.01), which means that it nearly captures  
326 the observed peak. Overall, the ‘SD-Box’ method yielded average scores of 1.18 for the  
327 peak stages and 1.08 for the peak times. In comparison with the ‘IQR-Box’ method,  
328 which yielded scores of 2.06 for the peak stages and 2.06 for the peak times, the results  
329 show that the enveloping rectangles defined using the ‘SD-Box’ method are more  
330 reliable during typhoon events.

331 *5.4 Including all forecasts with different lead times during an event to expand the*  
332 *sample size*

333 The sample size has a strong effect in terms of determining whether a result is  
334 statistically significant. In other words, the number of available ensemble members is  
335 important for both the ‘SD-Box’ and ‘IQR-Box’ methods. For example, the number of  
336 available ensemble members for each forecast ranged from 11 to 14 for the proposed



337 HEPS during operation. Thus, the descriptive statistics were calculated using  
338 insufficient sample sizes (less than 30). The same issue exists in other studies that  
339 employ HEPSs (e.g., Yang and Yang, 2014; Zappa et al., 2013). It is difficult to increase  
340 the number of ensemble members used in HEPSs, due to the limited computational  
341 resources that are available. Therefore, this study proposes a method for including  
342 present and previous forecasts in order to expand the sample size during the estimation  
343 process.

344 It must be shown that the forecast performance is independent of time before all  
345 available forecasts can be included in the estimation process. The time of concentration  
346 of the peak flow at the Zhongshan Bridge is approximately 4 hours. This study  
347 calculated the error in the maximum 4-hour rainfall between the average forecasts and  
348 the average observations at the watershed upstream of the Zhongshan Bridge. Figure 7  
349 shows that there is no obvious trend in the errors in stage and timing, regardless of the  
350 length of the lead time. The correlation coefficients were -0.09 and 0.11, respectively,  
351 and these values indicate that no significant correlations exist between errors in stage  
352 or timing on the one hand and lead time on the other. For example, the best and worst  
353 forecasts during Typhoon Dujuan in terms of stage error were the 1<sup>st</sup> and 5<sup>th</sup> forecasts,  
354 respectively. However, the 6<sup>th</sup> forecast was better than the 5<sup>th</sup>, which implies that there  
355 is no trend in the cascading forecasting process. Based on these results, this study



356 assumed that the performance of the HEPS is independent of lead time during typhoon  
357 events. Therefore, it is reasonable to include all available forecasts during an event to  
358 expand the sample size.

359 Figure 8 illustrates the comparisons between using the ‘SD-Box’ method with one  
360 forecast and using the ‘SD-Box’ method including all available forecasts (hereinafter  
361 indicated as ‘SD-Box Single’ and ‘SD-Box All’) at the Zhongshan Bridge. The  
362 performance of ‘SD-Box All’ was more consistent than that of ‘SD-Box Single’ in terms  
363 of both stage and timing. For example, the scores for stage during Typhoon Soudelor  
364 ranged from 0 to 5 when the ‘SD-Box Single’ method was used, but they were below  
365 or close to 1 with ‘SD-Box All’. The results showed that the inclusion of all available  
366 forecasts in the calculation process decreased the variation among the forecasts; in other  
367 words, the uncertainty of the forecasts decreased. Figure 9 illustrates the scores of all  
368 of the forecasts for the different typhoon events. The ‘SD-Box Single’ contained 47.1%  
369 of the observed peaks in terms of stage (37.3% + 9.8%), whereas ‘SD-Box All’  
370 contained 63.7% (57.8% + 5.9%) of the observed peaks. Furthermore, the ‘SD-Box  
371 Single’ contained 58.9% (37.3% + 21.6%) of the observed peaks in terms of timing,  
372 whereas ‘SD-Box All’ contained 71.5% (57.8% + 13.7%). The results show that the  
373 ‘SD-Box All’ method can capture more of the observed peaks in terms of both stage



374 and timing. In particular, ‘SD-Box All’ improved the forecast performance and  
375 increased the capture rate from 37.3% to 57.8% for both stage and timing.

## 376 6. CONCLUSIONS

377 This study proposed a HEPS that employs NWP models to perform rainfall  
378 forecasts and hydrologic models to produce ensemble flood forecasts during typhoon  
379 events. Because the communication of ensemble forecasts is critical for helping end-  
380 users to respond, a modified version of the ‘Peak-Box’ visualization method, which was  
381 originally described by Zappa et al. (2013), was also proposed to support the  
382 interpretation of ensemble forecast results for operational purposes. Four typhoon  
383 events during the period 2012-2015 and observations collected in the Yilan  
384 Experimental Watershed were used to evaluate the performance of these techniques. A  
385 total of 93 forecasts and two performance measures were considered. The results  
386 showed that the proposed HEPS is able to provide flood forecasts during the selected  
387 typhoon events. In addition, the ‘SD-Box’ visualization approach, which considers the  
388 mean and the standard deviation instead of the 25th and 75th percentiles, captured more  
389 of the observed peaks during typhoon events. The average skill-spread scores of the  
390 ‘SD-Box’ method for the selected events were 1.18 and 1.08 in terms of stage and  
391 timing, respectively. These results represent a significant improvement over the original  
392 ‘Peak-Box’ method, which resulted in scores of 2.06 for both peak stage and peak



393 timing. Scores of less than one indicate that the spread of the ensemble forecasts is large  
394 enough to contain the prediction uncertainty. Since the average score achieved by the  
395 ‘SD-Box’ method was close to one, it has been shown to be more reliable than the  
396 original ‘Peak-Box’ method during typhoon events. The results satisfy the statement  
397 “One of the main objectives of ensemble flood forecasts is the representation of the full  
398 spectrum of forecast uncertainty and/or predictability in [the] form of different  
399 hydrological responses to the input of the various members obtained from an  
400 atmospheric EPS” made by Zappa et al. (2013).

401 Descriptive statistics, such as the quartile deviation and the standard deviation, are  
402 susceptible to outliers when calculated using an insufficient number of observations.  
403 Adding more ensemble members is expensive in terms of computer resources. This  
404 study proposed a method that enables increasing the sample size, leading to statistically  
405 significant results. This method involves including present and previous available  
406 forecasts in the calculation process. For example, the proposed HEPS generated 11  
407 available ensemble members at each forecast during Typhoon Dujan. By including all  
408 of the present and previous available forecasts (the ‘SD-Box All’ method), the sample  
409 size increased to 22 for the second forecast, 33 for the third forecast, and so on. The  
410 results showed that the ‘SD-Box All’ made more consistent predictions. This result can  
411 be explained by the inclusion of all available forecasts in the calculation process



412 decreasing the uncertainty of the forecasts. As a result, the rectangles defined by the  
413 'SD-Box All' method contained 57.8% of the observed peaks in stage and timing.  
414 Coughlan de Perez et al. (2016) suggested that a HEPS that produces a false alarm rate  
415 below 50% is tolerable for decision makers in terms of the economic and practical  
416 consequences of taking action. However, this study assumed that the forecast  
417 performance of the proposed HEPS is independent of the length of the lead time and  
418 conducted an experiment to prove it. Other studies, such as that of Zappa et al. (2013),  
419 have claimed that the most accurate forecasts were obtained for lead times of two or  
420 more days. Such statements imply that the performance of HEPSs do not improve with  
421 shorter lead times or are independent of lead time, and Yang et al. (2016) found that the  
422 best performance is obtained before a typhoon makes landfall. This assumption is still  
423 susceptible to the topography of the applied area and the type of extreme event being  
424 considered. Further investigation of various conditions must be performed before firm  
425 conclusions can be drawn. Regardless, the proposed HEPS and the modified  
426 visualization approach have been shown to produce convincing peak-stage and peak-  
427 timing forecasts for operational purposes during a typhoon.

#### 428 AUTHOR CONTRIBUTION

429 Ya-Chi Chang, Mei-Ying Lin, Jui-Yi Ho calibrated and verified the parameters of  
430 WASH123D, POM and KW-GIUH models. Cheng-Hsin Chen dealt with the data  
431 processing of the models and performed the simulations. Sheng-Chi Yang and Ya-Chi



432 Chang analyzed the results of HEPS and developed a new approach for improved  
433 interpretation during typhoon events. Sheng-Chi Yang, Tsun-Hua Yang, Ya-Chi Chang  
434 and Kwan-Tun Lee prepared the manuscript with contributions from all co-authors.

#### 435 ACKNOWLEDGMENTS

436 The authors thank the Water Resources Agency of Taiwan for providing the  
437 hydrological observations from the rainfall gauges and water level stations in the Yilan  
438 River Basin. Thanks are also due to the Taiwan Typhoon and Flood Research Institute  
439 and the National Applied Research Laboratories for providing the results from the  
440 Taiwan Cooperative Precipitation Ensemble Forecast Experiment and historical records  
441 from the Yilan Experimental Watershed. This work was supported by the Ministry of  
442 Science and Technology, R.O.C., under grant MOST 105-3011-F-492-009.

#### 443 REFERENCES

- 444 Bartholmes, J. C., Thielen, J., Ramos, M. H., and Gentilini, S.: The european flood alert  
445 system EFAS-Part 2: Statistical skill assessment of probabilistic and deterministic  
446 operational forecasts, *Hydrology and Earth System Sciences*, 13, 141-153, 2009.
- 447 Blumberg, A. F. and Mellor, G. L.: A Description of a Three-Dimensional Coastal  
448 Ocean Circulation Model, in *Three-Dimensional Coastal Ocean Models*,  
449 American Geophysical Union, Washington, D.C., 1987.
- 450 Bruen, M., Krahe, P., Zappa, M., Olsson, J., Vehvilainen, B., Kok, K., and Daamen, K.:  
451 Visualizing flood forecasting uncertainty: some current European EPS platforms-  
452 COST731 working group 3, *Atmospheric Science Letters*, 11, 92-99, 2010.
- 453 Chiou, M. D.: Characteristic and numerical simulation of astronomic tide and storm  
454 surge in Taiwan water, Ph. D., Department of Hydraulic and Ocean Engineering,  
455 National Cheng Kung University, Tainan, Taiwan, 135 pp., 2010.
- 456 Cloke, H. L. and Pappenberger, F.: Ensemble flood forecasting: A review, *J. Hydrol.*,  
457 375, 613-626, 2009.
- 458 Coughlan de Perez, E., van den Hurk, B., van Aalst, M. K., Amuron, I., Bamanya, D.,  
459 Hauser, T., Jongman, B., Lopez, A., Mason, S., Mender de Suarez, J.,





- 460 Pappenberger, F., Rueth, A., Stephens, E., Suarez, P., Wagemaker, J., and Zsoter,  
461 E.: Action-based flood forecasting for triggering humanitarian action, *Hydrology  
462 and Earth System Sciences*, 20, 3549-3560, 2016.
- 463 Cuo, L., Pagano, T.C. and Wang, Q.J.: A review of quantitative precipitation forecasts  
464 and their use in short-to medium-range streamflow forecasting, *12*, 713-728, 2011.
- 465 Demeritt, D., Cloke, H., Pappenberger, F., Thielen, J., Bartholmes, J., and Ramos, M.-  
466 H.: Ensemble predictions and perceptions of risk, uncertainty, and error in flood  
467 forecasting, *Environmental Hazards*, 7, 115-127, 2007.
- 468 Demeritt, D., Nobert, S., Cloke, H., and Pappenberger, F.: Challenges in  
469 communicating and using ensembles in operational flood forecasting,  
470 *Meteorological applications*, 17, 209-222, 2010.
- 471 Frick, J. and Hegg, C.: Can end-users' flood management decision making be improved  
472 by information about forecast uncertainty?, *Atmospheric Research*, 100, 296-303,  
473 2011.
- 474 Fundel, F. and Zappa, M.: Hydrological ensemble forecasting in mesoscale catchments:  
475 Sensitivity to initial conditions and value of reforecasts, *Water Resources  
476 Research*, 47, W09520, 2011.
- 477 Hostache, R., Matgen, P., Montanari, A., Montanari, M., Hoffmann, L., and Pfister, L.:  
478 Propagation of uncertainties in coupled hydro-meteorological forecasting systems:  
479 A stochastic approach for the assessment of the total predictive uncertainty,  
480 *Atmospheric Research*, 100, 263-274, 2011.
- 481 Hsiao, L. F., Yang, M. J., Lee, C. S., Kuo, H. C., Shih, D. S., Tsai, C. C., Wang, C. J.,  
482 Chang, L. Y., Chen, D. Y. C., and Feng, L.: Ensemble forecasting of typhoon  
483 rainfall and floods over a mountainous watershed in Taiwan, *J. Hydrol.*, 506, 55-  
484 68, 2013.
- 485 Huang Jr, C., Yu, C. K., Lee, J. Y., Cheng, L. W., Lee, T. Y., and Kao, S. J.: Linking  
486 typhoon tracks and spatial rainfall patterns for improving flood lead time  
487 predictions over a mesoscale mountainous watershed, *Water Resources Research*,  
488 48, 2012.
- 489 Jang, J. H., Yu, P. S., Yeh, S. H., Fu, J. C., and Huang, C. J.: A probabilistic model for  
490 real-time flood warning based on deterministic flood inundation mapping,  
491 *Hydrological processes*, 26, 1079-1089, 2012.
- 492 Jaun, S., Ahrens, B., Walser, A., Ewen, T., and Schär, C.: A probabilistic view on the



- 493 August 2005 floods in the upper Rhine catchment, *Natural Hazards and Earth*  
494 *System Science*, 8, 281-291, 2008.
- 495 Kuo, C. W., Hong, J. H., Wang, H. W., Wang, Y. C., Tsun, S. C., and Li, S. C.:  
496 Comparisons of velocity profile extrapolation methods for moving-boat ADCP  
497 flow measurements, *Taiwan Water Conservancy*, 35-46, 2016.
- 498 Lee, K. T., Chang, C. H., Yang, M. S., and Yu, W. S.: Reservoir attenuation of floods  
499 from ungauged watersheds, *Hydrological Sciences Journal*, 46, 349-362, 2001.
- 500 Lee, K. T., Chung, Y. R., Lau, C. C., Meng, C. C., and Chiang, S.: A windows-based  
501 inquiry system for design discharge based on geomorphic runoff modeling,  
502 *Computers and Geosciences*, 32, 203-211, 2006.
- 503 Lee, K. T. and Yen, B. C.: Geomorphology and kinematic-wave-base hydrograph  
504 derivation, *Journal of Hydraulic Engineering ASCE*, 123, 73-80, 1997.
- 505 Li, M. H., Yang, M. J., Soong, R., and Huang, H. L.: Simulating typhoon floods with  
506 gauge data and mesoscale-modeled rainfall in a mountainous watershed, *Journal*  
507 *of Hydrometeorology*, 6, 306-323, 2005.
- 508 Ou, S., Liu, J., Tsai, C., and Hsu, T.: Numerical studies of typhoon-induced storm surge  
509 using POM and finite element depth-averaged model in Taiwan, *Chinese-German*  
510 *Joint Symposium on Hydraulic and Ocean Engineering*, Darmstadt, 2008.
- 511 Pagano, T. C., Wood, A. W., Ramos, M.-H., Cloke, H. L., Pappenberger, F., Clark, M.  
512 P., Cranston, M., Kavetski, D., Mathevet, T., and Sorooshian, S.: Challenges of  
513 operational river forecasting, *Journal of Hydrometeorology*, 15, 1692-1707, 2014.
- 514 Palmer, T. N.: A nonlinear dynamical perspective on model error: A proposal for non-  
515 local stochastic-dynamic parametrization in weather and climate prediction  
516 models, *Quarterly Journal of the Royal Meteorological Society*, 127, 279-304,  
517 2001.
- 518 Pappenberger, F., Beven, K. J., Hunter, N. M., Bates, P. D., Gouweleeuw, B. T., Thielen,  
519 J., and de Roo, A. P. J.: Cascading model uncertainty from medium range weather  
520 forecasts (10 days) through a rainfall-runoff model to flood inundation predictions  
521 within the European Flood Forecasting System (EFFS), *Hydrology and Earth*  
522 *System Sciences*, 9, 381-393, 2005.
- 523 Pappenberger, F., Cloke, H. L., Persson, A., and Demeritt, D.: HESS Opinions On  
524 forecast (in)consistency in a hydro-meteorological chain: curse or blessing?,  
525 *Hydrology and Earth System Sciences*, 15, 2011.



- 526 Pappenberger, F., Stephens, E., Thielen, J., Salamon, P., Demeritt, D., van Andel, S. J.,  
527 Wetterhall, F., and Alfieri, L.: Visualizing probabilistic flood forecast information:  
528 expert preferences and perceptions of best practice in uncertainty communication,  
529 Hydrological Processes, 27, 132-146, 2013.
- 530 Ramos, M. H., Mathevet, T., Thielen, J., and Pappenberger, F.: Communicating  
531 uncertainty in hydro - meteorological forecasts: mission impossible?,  
532 Meteorological Applications, 17, 223-235, 2010.
- 533 Renard, B., Kavetski, D., Kuczera, G., Thyer, M., and Franks, S. W.: Understanding  
534 predictive uncertainty in hydrologic modeling: The challenge of identifying input  
535 and structural errors, Water Resources Research, 46, W05521, 2010.
- 536 Rossa, A., Liechti, K., Zappa, M., Bruen, M., Germann, U., Haase, G., Keil, C., and  
537 Krahe, P.: The COST 731 Action: A review on uncertainty propagation in  
538 advanced hydro-meteorological forecast systems, Atmospheric Research, 100,  
539 150-167, 2011.
- 540 Shih, D. S., Yeh, G. T., and Cheng, J. R. C.: Model assessments of precipitation with a  
541 unified regional circulation rainfall and hydrological watershed model, Journal of  
542 Hydrologic Engineering ASCE, 17, 43-54, 2012.
- 543 Thielen, J., Bartholmes, J., Ramos, M. H., and de Roo, A. P. J.: The European Flood  
544 Alert System; Part 1: Concept and development, Hydrology and Earth System  
545 Sciences, 13, 125-140, 2009.
- 546 Thiessen, A. H.: Precipitation averages for large areas, Monthly Weather Review, 39,  
547 1082-1084, 1911.
- 548 Thirel, G., Martin, E., Mahfouf, J. F., Massart, S., Ricci, S., and Habets, F.: A past  
549 discharges assimilation system for ensemble streamflow forecasts over France-  
550 Part 1: Description and validation of the assimilation system, Hydrology and Earth  
551 System Sciences, 14, 1623-1637, 2010.
- 552 Todini, E.: Predictive uncertainty assessment in real time flood forecasting. In:  
553 Uncertainties in Environmental Modelling and Consequences for Policy Making,  
554 Baveye, P. C., Laba, M., and Mysiak, J. (Eds.), Springer, Dordrecht, Netherlands,  
555 2009.
- 556 Wilks, D. S.: Statistical Methods in the Atmospheric Sciences, Elsevier, Amsterdam,  
557 2006.
- 558 Yang, S. C. and Yang, T. H.: Uncertainty assessment: Reservoir inflow forecasting with

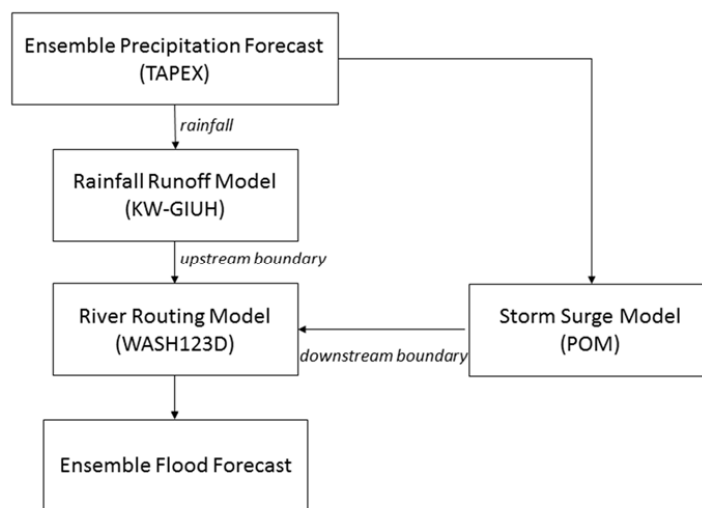


- 559 ensemble precipitation forecasts and HEC-HMS, *Advances in Meteorology*, 2014,  
560 2014.
- 561 Yang, T. H., Hwang, G. D., Tsai, C.-C., and Ho, J.-Y.: Using rainfall thresholds and  
562 ensemble precipitation forecasts to issue and improve urban inundation alerts,  
563 *Hydrology and Earth System Sciences*, 20, 4731, 2016.
- 564 Yeh, G. T., Cheng, H. P., Cheng, J. R., and Lin, J. H.: A numerical model to simulate  
565 flow and contaminant and sediment transport in watershed systems (WASH12D).  
566 Technical Rep. CHL-98-15, Waterways Experiment Station, U. S. Army Corps of  
567 Engineers, Vicksburg, MS 39180-6199., 1998. 1998.
- 568 Yeh, G. T., Huang, G. B., Zhang, F., Cheng, H. P., and Lin, H. C.: WASH123D: A  
569 numerical model of flow, thermal transport, and salinity, sediment, and water  
570 quality transport in watershed systems of 1-D stream-river network, 2-D overland  
571 regime, and 3-D subsurface media. Technical Rep. submitted to EPA, Dept. of  
572 Civil and Environmental Engineering, 2006.
- 573 Yeh, G. T., Shih, D. S., and Cheng, J. R. C.: An integrated media, integrated processes  
574 watershed model, *Computers and Fluids*, 45, 2-13, 2011.
- 575 Zappa, M., Beven, K. J., Bruen, M., Cofino, A. S., Kok, K., Martin, E., Nurmi, P.,  
576 Orfila, B., Roulin, E., Schroter, K., Seed, A., Szturc, J., Vehvilainen, B., Germann,  
577 U., and Rossa, A.: Propagation of uncertainty from observing systems and NWP  
578 into hydrological models: COST-731 Working Group 2, *Atmospheric Science*  
579 *Letter*, 11, 83-91, 2010.
- 580 Zappa, M., Fundel, F., and Jaun, S.: A 'Peak-Box' approach for supporting interpretation  
581 and verification of operational ensemble peak-flow forecasts, *Hydrological*  
582 *Processes*, 27, 117-131, 2013.
- 583 Zappa, M., Jaun, S., Germann, U., Walser, A., and Fundel, F.: Superposition of three  
584 sources of uncertainties in operational flood forecasting chains, *Atmospheric*  
585 *Research*, 100, 246-262, 2011.



586

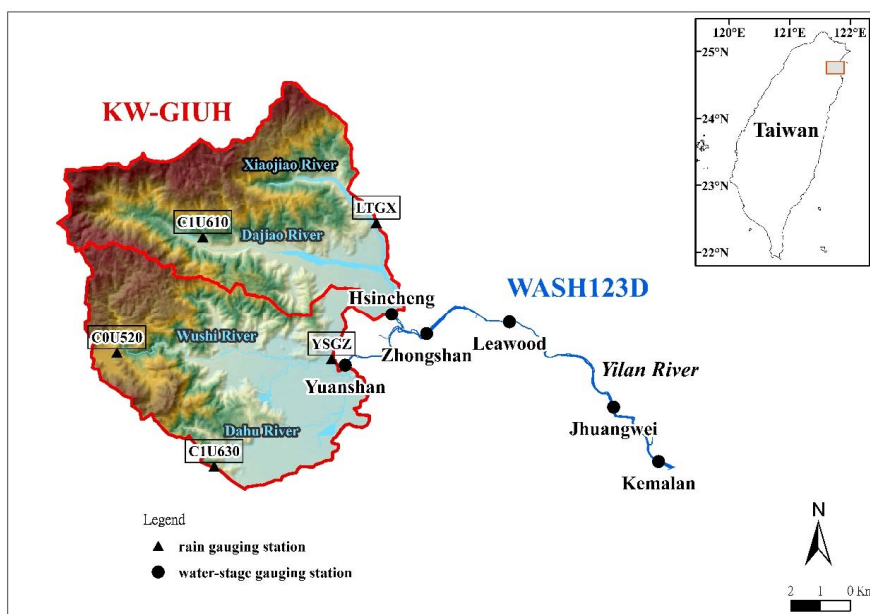
## FIGURES



587

588 **Figure 1** Flowchart describing the flow of data processing within the Yilan River  
589 HEPS.

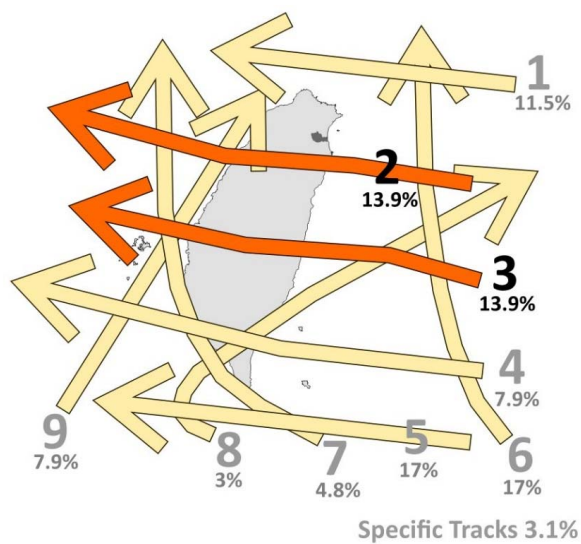
590



591

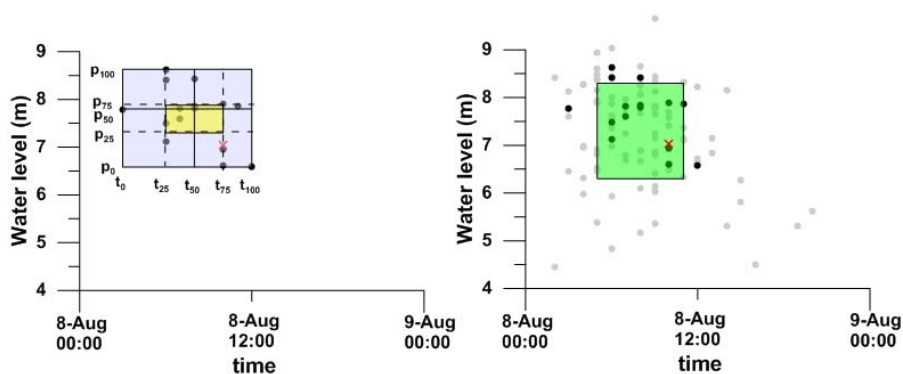
592 **Figure 2** Study area and locations of streamflow gauges. Black dots and triangles  
593 indicate the locations of water-stage gauging stations and rain gauge stations,  
594 respectively.

595



Redrawn from Kuo et al. (2012)

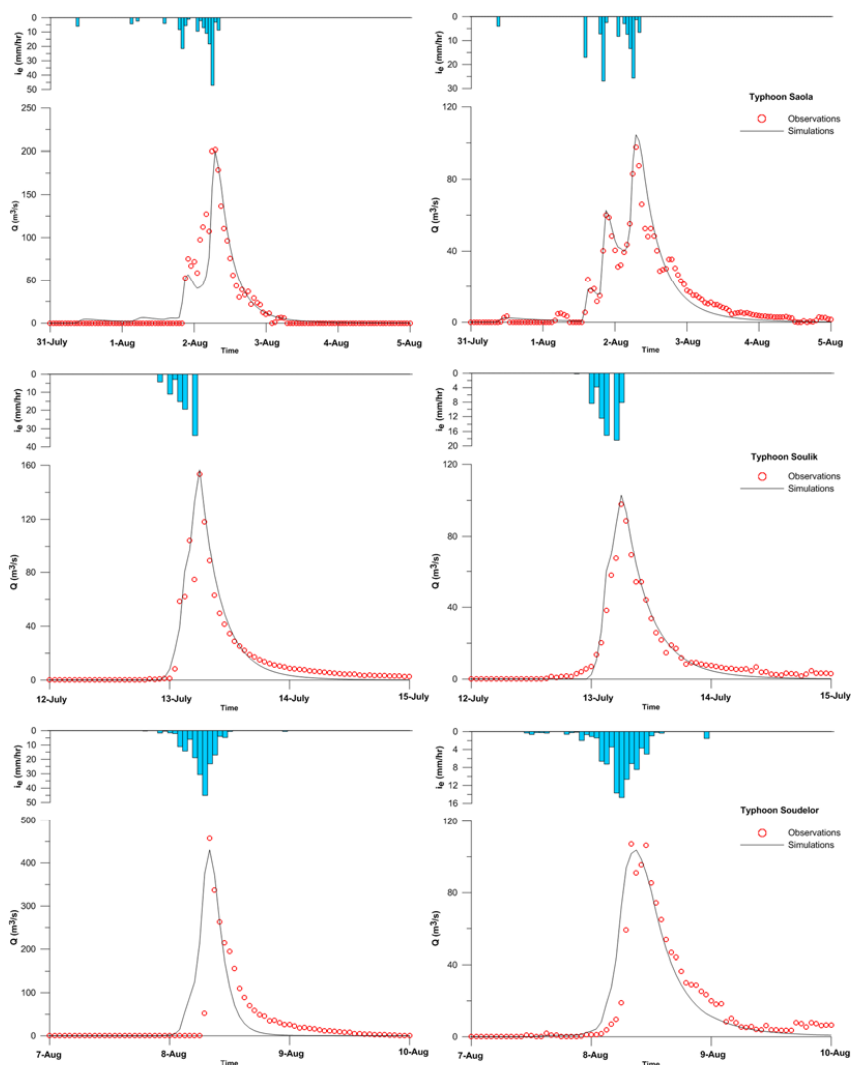
596 **Figure 3** Schematic diagram showing the tracks of typhoons invading Taiwan. The  
597 percentages shown in the figure are the statistical results from 1958 through 2006  
598 obtained from the Central Weather Bureau (CWB). The dark gray polygon located in  
599 northern Taiwan indicates the Yilan River catchment. Type-2 and Type-3 typhoons  
600 bring heavy rainfall to the Yilan River catchment.



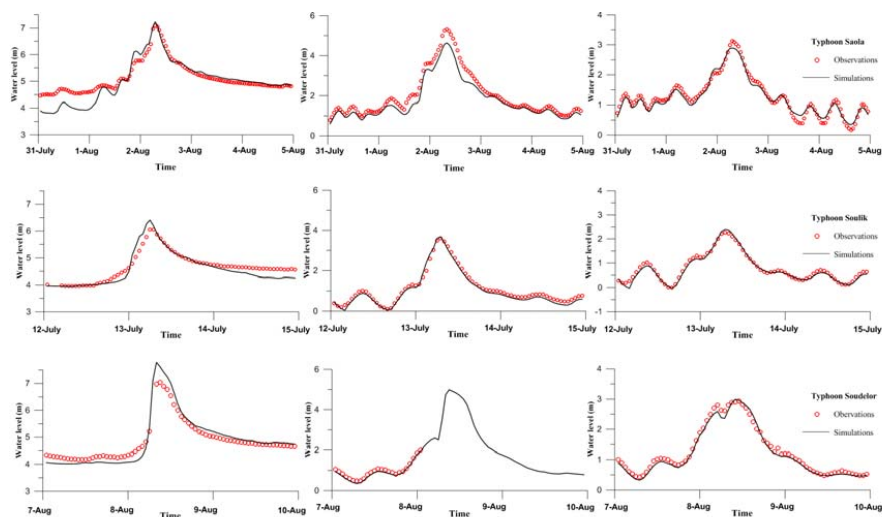
601

602 **Figure 4** The left panel shows a graphical explanation of the 'Peak-Box' approach.  
603 The outer rectangle is the 'Peak-Box,' and the internal rectangle (the yellow area) is  
604 the 'IQR-Box'. The solid dots represent all of the ensemble forecasts. The right panel  
605 shows a graphic explanation of the proposed extension of the 'Peak-Box' approach.  
606 The enveloping rectangle is the 'SD-Box' (the green area). The solid black and gray  
607 dots represent current and previous peak-flow forecasts, respectively.





608 **Figure 5** Comparison of simulated discharges (red circles) and recorded discharges  
609 (solid lines) for model calibration (Typhoons Saola and Soulik) and validation  
610 (Typhoon Soudelor) experiments at Hsinsheng (left) and Yuanshen (right). The blue  
611 bars are the hourly spatial-average rainfall intensities measured in the watershed  
612 upstream of Hsinsheng and Yuanshen.

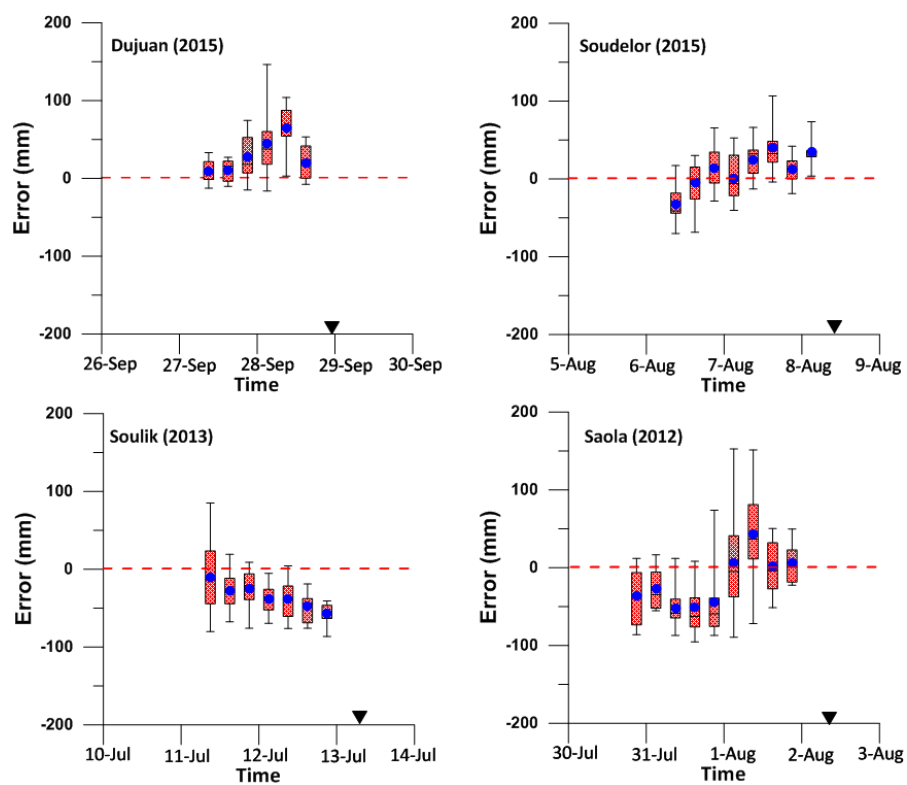


613

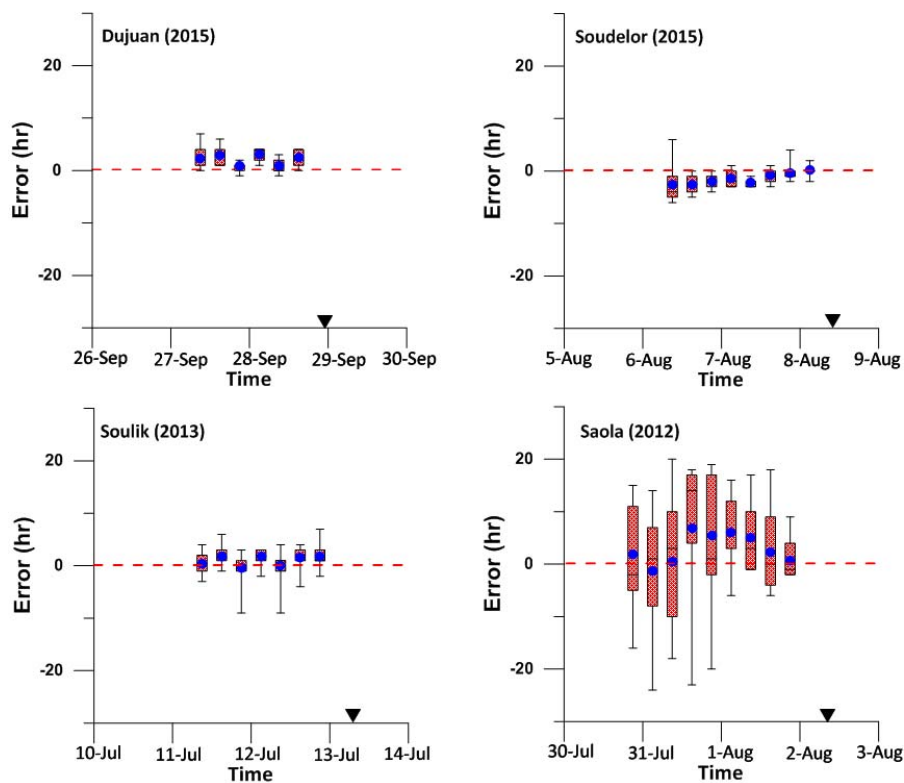
614 **Figure 6** Comparison of simulated (red circles) and recorded (solid lines) water levels  
615 for model calibration (Typhoons Saola and Soulik) and validation (Typhoon Soudelor)  
616 experiments at Zhongshan (left), Leawood (center) and Jhungwei (right).



**(a) Magnitude error of maximum 4-hour rainfall**



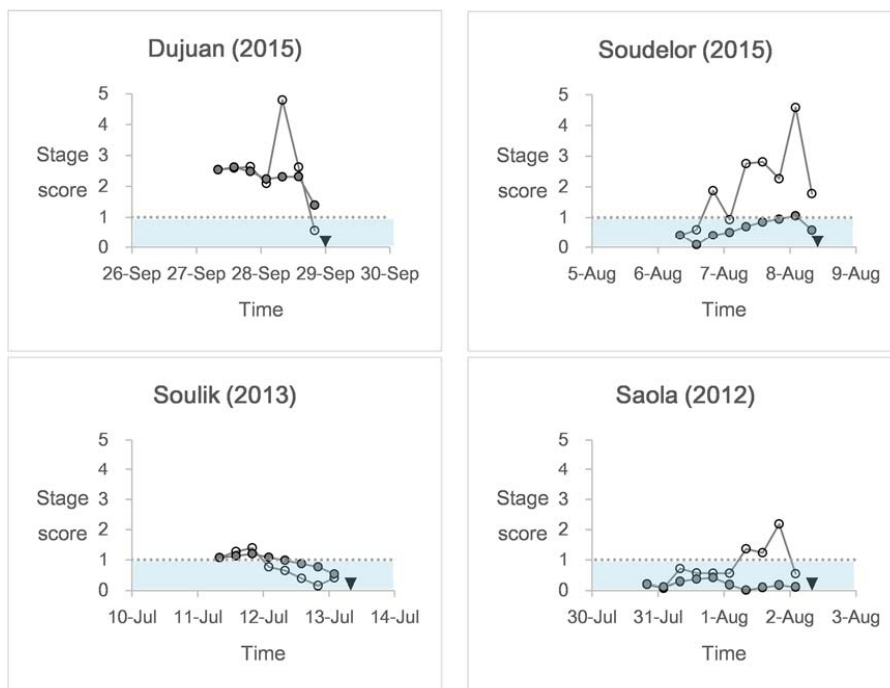
**(b) Timing error of maximum 4-hour rainfall**



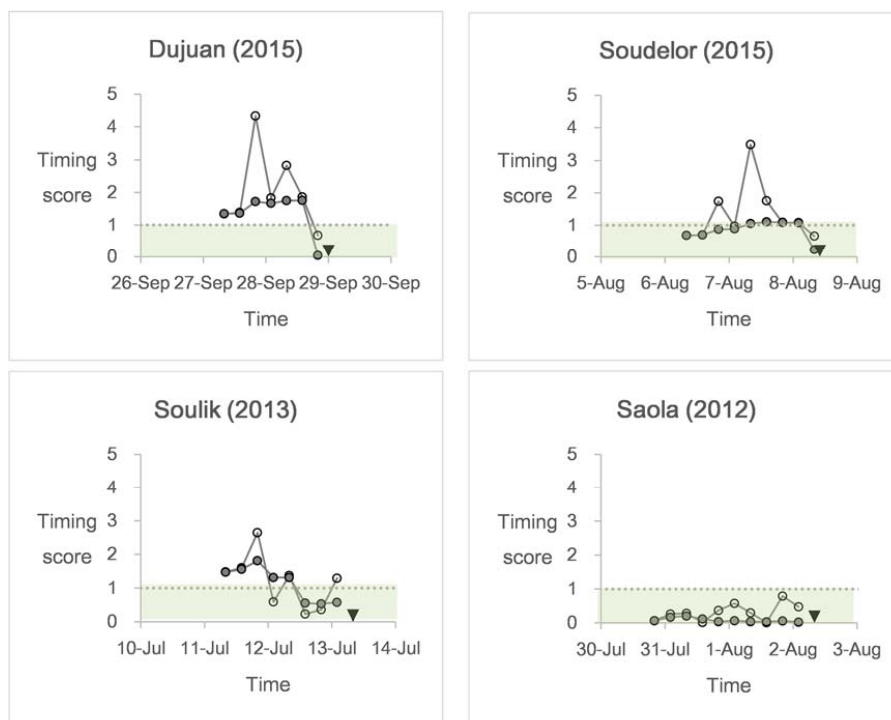
617 **Figure 7** Box-and-whisker plot at the watershed upstream of the Zhongshan Bridge  
618 during the four selected typhoon events. The blue dots indicate the ensemble means.  
619 The inverted triangles indicate the time of occurrence of the maximum 4-hour rainfall.  
620 The results show that there is no obvious trend in lead time for the errors in either the  
621 stage or timing.



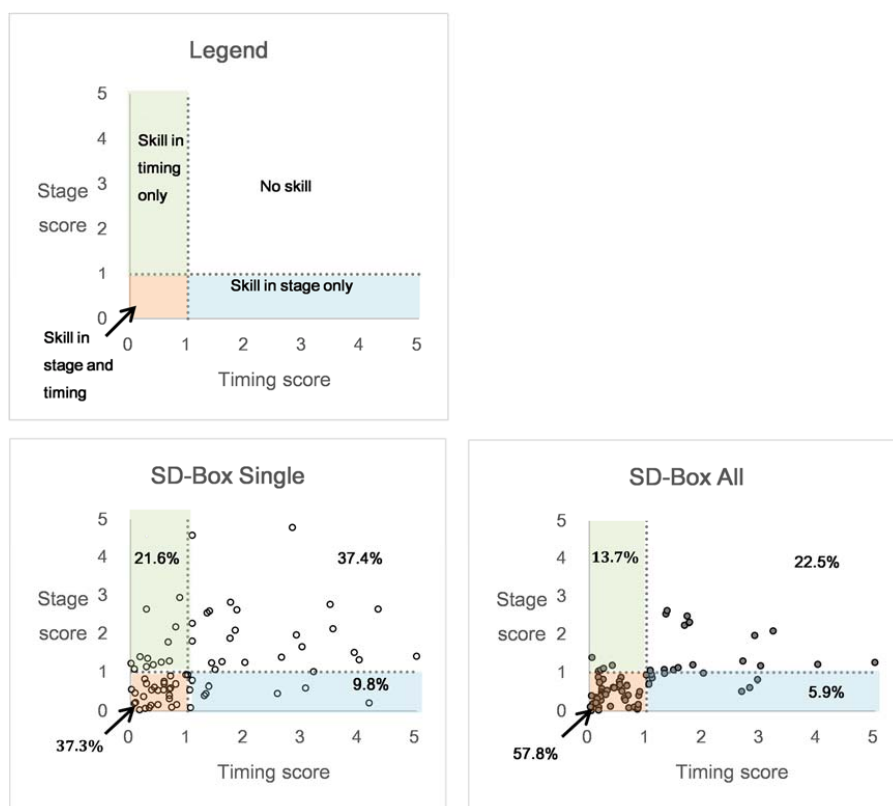
**(a) Scores for peak-stage forecasts**



**(b) Scores in peak-timing forecasts**



622 **Figure 8** The scores of the single ('SD-Box Single') and accumulating ('SD-Box All')  
623 methods at the Zhongshan Bridge during the four selected typhoon events. The inverted  
624 triangles indicate the time of occurrence of the observed peak stage. The results show  
625 that the performance of the 'SD-Box All' method (solid circles) was more stable than  
626 that of the 'SD-Box Single' method (open circles) in terms of both stage and timing.  
627



628

629 **Figure 9** Comparison of scores obtained for ‘SD-Box Single’ and ‘SD-Box All’. The  
 630 results show that the ‘SD-Box All’ approach significantly improves the performance  
 631 compared with the results obtained using the ‘SD-Box Single’ method.



632

## TALBLES

633 **Table 1** All typhoons that invaded Taiwan during 2012 through 2015. A total of four  
 634 typhoons of Type-2 and Type-3, namely, Saola in 2012, Soulik in 2013, Soudelor in  
 635 2015, and Dujuan in 2015, were selected to calibrate the system and test the  
 636 performance in this study. Typhoon Matmo, a Type-3 typhoon that occurred in 2014,  
 637 was not selected due to its weak typhoon intensity.

Typhoon	Track	Intensity	Warning Period
DUJUAN	2	3	27-29 September 2015
GONI	—	—	20-23 August 2015
SOUDELOR	3	3	6-9 August 2015
LINFA	—	—	6-9 July 2015
CHAN-HOM	—	2	9-11 July 2015
NOUL	—	—	10-11 May 2015
FUNG-WONG	Special	—	19-22 September 2014
MATMO	3	—	21-23 July 2014
HAGIBIS	—	3	14-15 Jun 2014
FITOW	1	—	4-7 October 2014
USAGI	5	3	19-22 September 2013
KONG-REY	6	—	27-29 August 2013
TRAMI	1	—	20-22 August 2013
CIMARON	—	—	17-18 July 2013
SOULIK	2	1	11-13 July 2013
JELAWAT	—	—	27-28 September 2012
TEMBIN	Special	—	21-25 August 2012
		—	26-28 August 2012
KAI-TAK	—	1	14-15 August 2012
HAIKUI	—	—	6-7 August 2012
SAOLA	2	4	30 July - 3 August 2012
DOKSURI	—	—	28-29 Jun 2012
TALIM	9	—	19-21 Jun 2012

638

(Source: Central Weather Bureau, Taiwan)





639 **Table 2** Comparisons of scores in peak stage and peak time between the ‘IQR-Box’  
 640 and ‘SD-Box’ approaches. Scores less than one (highlighted) indicate that the  
 641 enveloping rectangle did contain the observed peak.

642 **(a) Scores in peak-stage forecasts**

Location/Typhoon	Method	Forecast									
		1	2	3	4	5	6	7	8	9	10
<b>Zhongshan Bridge</b>											
Dujuan (2015)	SD-Box	2.54	2.59	2.64	2.09	4.79	2.62	0.57	–	–	–
	IQR-Box	2.83	3.78	3.30	4.53	14.03	2.87	1.07	–	–	–
Soudelor (2015)	SD-Box	0.41	0.60	1.88	0.93	2.76	2.82	2.27	4.59	1.78	–
	IQR-Box	0.22	1.26	2.20	1.14	3.39	7.00	4.07	10.60	2.58	–
Soulik (2013)	SD-Box	1.07	1.27	1.39	0.76	0.64	0.38	0.15	0.40	–	–
	IQR-Box	1.86	1.76	1.94	1.29	0.87	0.36	0.65	0.56	–	–
Saola (2012)	SD-Box	0.20	0.07	0.71	0.56	0.55	0.55	1.36	1.23	2.18	0.54
	IQR-Box	0.14	0.01	1.81	0.79	1.70	1.42	3.66	1.90	2.45	0.48
<b>Leawood Bridge</b>											
Dujuan (2015)	SD-Box	1.21	1.27	1.75	1.24	3.48	1.48	1.67	–	–	–
	IQR-Box	1.10	2.29	2.17	2.98	11.15	1.84	3.23	–	–	–
Soudelor (2015)	SD-Box	–	–	–	–	–	–	–	–	–	–
	IQR-Box	–	–	–	–	–	–	–	–	–	–
Soulik (2013)	SD-Box	0.79	0.95	1.06	0.36	0.20	0.10	0.27	0.54	–	–
	IQR-Box	1.76	1.79	2.06	0.75	0.31	0.16	0.09	0.76	–	–
Saola (2012)	SD-Box	0.93	1.25	1.66	1.32	1.41	0.16	0.29	0.22	0.04	1.36
	IQR-Box	1.14	2.12	2.71	1.60	2.51	0.00	1.32	0.01	0.28	1.36
<b>Zhuangwei Bridge</b>											
Dujuan (2015)	SD-Box	1.97	2.13	0.60	0.21	0.46	1.51	2.94	–	–	–
	IQR-Box	2.76	2.88	0.73	0.35	1.62	1.93	4.29	–	–	–
Soudelor (2015)	SD-Box	1.19	0.17	0.45	0.10	1.01	1.24	0.55	1.81	2.64	–
	IQR-Box	1.47	0.23	0.31	0.00	0.87	3.30	0.85	3.03	3.69	–
Soulik (2013)	SD-Box	0.62	0.71	0.79	0.17	0.03	0.32	0.47	0.90	–	–
	IQR-Box	1.45	1.53	1.77	0.49	0.00	0.40	0.45	1.18	–	–
Saola (2012)	SD-Box	0.82	1.08	1.40	1.14	1.26	0.09	0.70	0.09	0.22	1.29
	IQR-Box	1.06	2.39	2.55	1.57	3.42	0.39	1.77	0.37	0.03	1.39



644 (b) Scores in peak-timing forecasts

Location/Typhoon	Method	Forecast									
		1	2	3	4	5	6	7	8	9	10
<b>Zhongshan Bridge</b>											
Dujuan (2015)	SD-Box	1.34	1.38	4.33	1.83	2.83	1.86	0.68	—	—	—
	IQR-Box	3.67	3.00	9.00	2.00	3.00	1.67	0.94	—	—	—
Soudelor (2015)	SD-Box	0.68	0.70	1.74	0.97	3.49	1.75	1.08	1.08	0.66	—
	IQR-Box	1.00	1.67	3.00	1.00	7.00	2.00	—	3.00	5.40	—
Soulik (2013)	SD-Box	1.48	1.60	2.64	0.59	1.37	0.23	0.36	1.29	—	—
	IQR-Box	3.00	3.57	4.00	1.00	2.00	1.00	1.00	2.33	—	—
Saola (2012)	SD-Box	0.07	0.26	0.28	0.02	0.37	0.58	0.30	0.01	0.79	0.48
	IQR-Box	0.10	0.29	0.81	0.18	0.67	1.14	0.33	0.11	1.00	0.56
<b>Leawood Bridge</b>											
Dujuan (2015)	SD-Box	0.46	0.11	1.69	0.32	2.24	0.58	0.71	—	—	—
	IQR-Box	1.00	0.33	3.00	0.20	3.00	0.60	1.00	—	—	—
Soudelor (2015)	SD-Box	—	—	—	—	—	—	—	—	—	—
	IQR-Box	—	—	—	—	—	—	—	—	—	—
Soulik (2013)	SD-Box	0.40	1.17	1.96	0.39	0.71	0.11	0.09	0.96	—	—
	IQR-Box	1.18	5.00	3.00	1.00	1.00	1.00	1.00	1.50	—	—
Saola (2012)	SD-Box	0.04	0.09	0.34	0.17	0.04	0.11	0.46	0.07	0.67	0.53
	IQR-Box	0.29	0.10	0.76	0.22	0.53	0.88	0.50	0.00	0.80	1.00
<b>Zhuangwei Bridge</b>											
Dujuan (2015)	SD-Box	2.90	3.54	3.06	4.17	2.57	3.91	0.86	—	—	—
	IQR-Box	6.33	11.00	5.00	7.00	3.00	4.20	1.13	—	—	—
Soudelor (2015)	SD-Box	0.40	0.48	1.32	0.72	3.20	1.42	1.04	1.08	0.28	—
	IQR-Box	0.50	1.00	1.67	1.00	3.00	2.00	3.00	3.00	0.00	—
Soulik (2013)	SD-Box	0.42	0.59	1.08	0.81	0.16	0.68	0.08	0.70	—	—
	IQR-Box	0.33	1.00	2.00	3.00	0.14	3.00	1.00	1.00	—	—
Saola (2012)	SD-Box	0.25	0.07	0.17	0.28	0.54	1.05	0.79	0.33	0.09	0.68
	IQR-Box	0.72	0.50	0.00	3.43	1.07	1.71	1.00	0.44	0.00	5.00

645